

The spatial statistics of structural magnetic resonance images: application to post-acquisition quality assessment of brain MRI images

M. E. Osadebey, Marius Pedersen, Douglas Arnold, Katrina Wendel-Mitoraj & The Alzheimer's Disease Neuroimaging Initiative

To cite this article: M. E. Osadebey, Marius Pedersen, Douglas Arnold, Katrina Wendel-Mitoraj & The Alzheimer's Disease Neuroimaging Initiative (2017) The spatial statistics of structural magnetic resonance images: application to post-acquisition quality assessment of brain MRI images, The Imaging Science Journal, 65:8, 468-483, DOI: [10.1080/13682199.2017.1369641](https://doi.org/10.1080/13682199.2017.1369641)

To link to this article: <https://doi.org/10.1080/13682199.2017.1369641>



Published online: 07 Sep 2017.



Submit your article to this journal [↗](#)




Article views: 74



View Crossmark data [↗](#)



The spatial statistics of structural magnetic resonance images: application to post-acquisition quality assessment of brain MRI images

M. E. Osadebey^a, Marius Pedersen^b, Douglas Arnold ^{c,d}, Katrina Wendel-Mitoraj^e and The Alzheimer's Disease Neuroimaging Initiative

^aMRI Reader Group, NeuroRx Research Inc., Montreal, Canada; ^bDepartment of Computer Science, Norwegian University of Science and Technology, Gjøvik, Norway; ^cNeuroRx Research Inc., Montreal, Quebec, Canada; ^dMontreal Neurological Institute, McGill University, Montreal, Canada; ^eBrainCare Oy, Tampere, Finland

ABSTRACT

This report describes a new quality evaluation method for structural magnetic resonance images (MRI) of the brain. Pixels in MRI images are regarded as regionalized random variables that exhibit distinct and organized geographic patterns. We extract geo-spatial local entropy features and build three separate Gaussian distributed quality models upon them using 250 brain MRI images of different subjects. The MRI images were provided by Alzheimer's disease neuroimaging initiative (ADNI). Image quality of a test image is predicted in a three-step process. In the first step, three separate geo-spatial feature vectors are extracted. The second step standardizes each quality model using corresponding geo-spatial feature vector extracted from the test image. The third step computes image quality by transforming the standardized score to probability. The proposed method was evaluated on images without perceived distortion and images degraded by different levels of motion blur and Rician noise as well as images with different configurations of bias fields. Based on the performance evaluation, our proposed method will be suitable for use in the field of clinical research where quality evaluation is required for the brain MRI images acquired from different MRI scanners and different clinical trial sites before they are fed into automated image processing and image analysis systems.

ARTICLE HISTORY

Received 20 June 2016
Accepted 14 August 2017

KEYWORDS

Magnetic resonance imaging; image quality; whole brain angular segment pixel density; transverse segment pixel density; whole brain pixel density and Gaussian distribution

1. Introduction

Evaluation of image quality is a preliminary post-acquisition step. The quality of image acquisition devices, the necessary post-acquisition processing procedures, performance evaluation of image processing and image analysis algorithms and the level of utility of an image are determined by the outcome of image quality evaluation. Strategic imaging work-flow decisions, such as choice of imaging device, algorithms for image processing and image analysis, re-scan, re-processing and re-analysis, are influenced by image quality evaluation. The extent to which a trained reader or an automated image analysis system can optimally extract the information contained in an image is determined by the image quality. Thus image quality assessment is a very important step in the process of utilization of an image.

The first step in the evaluation of image quality is the identification of manageable image quality attributes [1, 2]. These attributes expressed as quality features are then measured using different quality scores to obtain a total quality score referred to as an image quality index [3]. The goal of objective image quality evaluation is to derive an image quality metric which correlates with the evaluation by the human visual

system in terms of 'fidelity', 'usefulness' and 'naturalness' [4]. Image quality can be evaluated by humans in what is referred to as a subjective method [5] or by a measuring device in what is referred to as an objective method [2]. This paper focuses on how to quantify the diagnostic information contained in structural magnetic resonance images of the brain without any reference to an original image and such that the evaluation correlates with the human visual system.

Advances in image acquisition technology encouraged increasing interest in the use of magnetic resonance imaging (MRI) system images for the study of human anatomy [6, 7] diagnosis of diseases [8, 9] and the clinical trials of drugs for the treatment of neurological diseases [10–12]. The attractive feature of an MRI system is its potential to produce high-contrast images of soft anatomical structures. This potential is an ideal expectation because of the imperfections of the system components, trade-offs in system operating parameters, patient-induced artefact and operator error. The perceived visual quality of an MRI image of the brain is influenced by features that manifest in the image. The features include noise at different levels, intensity non-uniformity, acquisition artefacts, blurring, geometric distortion, lesion load and

extraneous artefacts introduced by image processing and image analysis algorithms [13]. These features influence each other as well as the classical terms of perception such as sharpness, contrast and saturation, and thus makes image quality evaluation a nontrivial task [2].

1.1. Literature review

Several objective image quality measures have been proposed in the literature. They can be categorized into reference or reduced reference methods [13–19] and no-reference methods [20–25]. A detailed review of image quality evaluation for a general class of images and MRI images can be found in [26–33]. Despite the several contributions on image quality, the popular quality assessment metrics for medical images are the age-old techniques: root-mean-square error (RMSE), signal-to-noise ratio (SNR) and structural similarity index (SSIM) [14]. These metrics were designed to solve research problems that were not related to image interpretation but on efficient compression, storage and transmission of images. We identified six drawbacks in current automated image quality assessment methods. They are explained as follows:

- (1) *Generalization of Medical Images.* The popular quality evaluation metrics assume that all classes of medical images and all other natural images have the same descriptive features. Medical images exhibit characteristics such as texture, grey-scale colour, noise and homogeneity that distinguish them from each other and other classes of natural images.
- (2) *Globalization.* Different structures of the brain respond differently to the same level of distortion. Quality assessments in [14, 15, 22–24] take into account the entire image and do not allow focus towards region-of-interest. In some clinical applications, such as the study of disease progression in multiple sclerosis, the focus is detection of lesions in the white matter region. The focus changes to the cortical grey matter region in cortical grey matter atrophy measurement and to the ventricle in ventricular atrophy measurement. With global quality measures, there is the risk of non-optimal quality measure in a region which is the focus of the physician or a trained reader.
- (3) *Distortion-Specific Bias.* Many current quality assessment methods, such as [20, 22], adopt specific type of distortion, considered as common, to evaluate the image under consideration. This approach can be said to be biased towards specific distortion, because all possible distortions combine with ideal features to manifest as image attribute [21].

- (4) *Fidelity Bias.* Image quality as viewed by the human visual system can be represented in three dimensions: fidelity, usefulness and naturalness. Researchers have argued that the use of reference images such as in [14] for quality evaluation is a measure of fidelity and does not account for the other two attributes of image quality.
- (5) *Limitations of Classical Statistics.* All the current quality assessment metrics adopt the principles of classical statistics to describe quality attributes. Classical statistics does not account for the distinct geographic patterns of the constituent anatomic structures in medical images. The absence of spatial dependence in the description of these attributes excludes the naturalness of the image in the evaluation of image quality. The inability of popular image quality measures to perceptually distinguish different images was reported in [16]. The authors demonstrated that two images with the same RMSE can be perceptually dissimilar. They proposed a technique called null space analysis for quality evaluation.

1.2. Importance of automated Objective quality measures

There are many real-world applications where there is little room to operate the human visual system method for the evaluation of image quality. A typical scenario is in clinical research organizations. Several thousands of brain MRI images are delivered daily from clinical trial sites around the globe to clinical research organizations that manage clinical trials of new drugs for pharmaceutical organizations. Variations in the quality of images acquired with different scanners from the different clinical trial sites need to be quantified to ensure conformity with the protocols set out by sponsoring pharmaceutical organizations. The method of transmission from the clinical trial sites and the image analysis systems within the clinical research organizations can introduce some amount of distortion or artefact into the images [13, 19]. Efficient management of this large amount of data demands high level of automation in the methods of quality assessment of the MRI images. There is little tolerance for subjective quality measures, because they are manual, time-consuming and lack repeatability. No-reference, objective and automatic quality measures are preferred, because they can be computed in real time and are repeatable. Objective quality measures encourage efficient data management by the classification of images for assignment of real-time automated processing, manual processing, further processing to improve image quality and the assessment of overall performance of image analysis systems [34].

1.3. Introduction to spatial statistics

Spatial statistics [35] is a branch of classical statistics. It is a relatively new area in statistics. It became an active research area because of the limitations of classical statistics to solve some real-world problems. There are three major techniques in spatial statistics. They are geostatistics, spatial point patterns and lattice data. For the purpose of this research, our interest is in the area of geostatistics. The Geostatistical technique focuses on fixed spatial region such as a geographical region for the modelling of continuous variables, data prediction from the relationship between variables and evaluation of spatial structures. It can distinguish the visual perception of images by incorporating information about their spatial dependences. Data from brain images acquired by MRI system have characteristics suitable for spatial analysis. Three-dimensional display of brain MRI image reveals clearly defined pattern in the spatial location and the spatial arrangement of the anatomical structures of the brain. The data are continuous variables describing different anatomic structures within a fixed spatial region. The nomenclature adopted for the acquisition planes and some of the constituent anatomic structures: axial, sagittal, coronal, left hemisphere, right hemisphere and mid-sagittal plane are borrowed from the field of geography to describe spatial locations within the brain. The spatial arrangement is the most important attribute of MRI image that is easily perceived by an observer. Every trained reader has the knowledge that the brain is approximately symmetrical with respect to the mid-sagittal plane, the lateral ventricle is approximately centred on the mid-sagittal plane and farther from the brain surface than the cortical grey matter [36, 37]. After a careful review of the literature, we can say that, to the best of our knowledge, there is yet no proposed method on the application of the principles of spatial statistics to the evaluation of image quality.

1.4. Proposed quality metric

We propose a new fully automated, no-reference, objective method to evaluate the quality of MRI system images. It is based on encoding different image quality attributes with local entropy. Entropy is a direct measure of the classical image quality attributes such as luminous brightness, contrast, sharpness, noise and texture [38]. Our proposed method also exploits the similarity in the geometry of human anatomy across age, gender and race [39–41]. The human brain is regarded to be located in a fixed spatial region that exhibits distinct and organized patterns. Three geographic regions are defined to extract spatial information from the whole brain, axial slices

and specific angular segments within slices in an MRI volume data. Three spatial quality models were built from brain MRI images of 250 subjects sourced from Alzheimer's disease neuroimaging initiative (ADNI) database.

1.5. Outline

This paper is organized as follows. The next section describes our methods for the evaluation of image quality. Performance evaluation of our proposed method is in Section 3. Experimental results are discussed in Section 4. Section 5 concludes this report.

2. Methods

2.1. Data and sources of data

The proposed method utilized data from three different sources. They are T1-weighted MRI images acquired using three-dimensional magnetization-prepared rapid gradient echo (MPRAGE) images from the ADNI database. The MPRAGE images constitute the model database. The performance evaluation of our proposed method was carried out using original MRI data from NeuroRx research Inc and BrainCare Oy.

The ADNI (<http://adni.loni.usc.edu/>) was launched in 2003 as a public–private partnership, led by the Principal Investigator Michael W. Weiner, MD. The primary goal of ADNI has been to test whether serial magnetic resonance imaging (MRI), positron emission tomography (PET), other biological markers, and clinical and neuropsychological assessment can be combined to measure the progression of mild cognitive impairment (MCI) and early Alzheimer's disease (AD). NeuroRx inc. (<https://www.neurorx.com>) is a clinical research organization dedicated to working with the pharmaceutical industry to facilitate clinical trials of new drugs for multiple sclerosis (MS) and other neurological diseases. BrainCare Oy (<http://braincare.fi/>) is a Tampere University of Technology spin-off company founded in 2013 to deliver personalized solutions to improve the quality of life of epilepsy patients. The organization recently concluded clinical trials for a novel mobile application and supporting solutions for long-term monitoring for epileptic patient.

Two hundred and fifty high-quality, high-resolution, 3D, T1-weighted MPRAGE MRI images were our choice for the model database, because images acquired using MPRAGE pulse sequence exhibit superior grey-white matter contrast compared to the conventional T1 and other structural brain MRI images [42–44]. Each slice has a thickness of 1.2 mm and a dimension of 190 × 160. Details of ADNI acquisition protocol and the initial processing steps are available in [45]. During data sourcing at ADNI website, we seek MRI

data of patients with healthy and normal brains that were without lesions or with very mild lesions. For each MRI data, slices towards the most inferior and most superior sections are discarded, because they highlight more of scalp and bone structures than brain structures. There are variations in the number of useful slices for different patients. For each patient data, the index of useful slices were coded in a special function which can be called up by the algorithm during the modelling experiment.

There are one original T1-weighted, one T2-weighted and one Fluid Attenuated Inverse Recovery (FLAIR) images from NeuroRx research Inc. All the data from NeuroRx has same slice thickness of 2.4 mm, dimension 256×256 and consist of 60 slices. The images were without perceived distortion except the T1-weighted images which were originally acquired with intensity inhomogeneity. The data from BrainCare Oy are one original T2-weighted data with high lesion load and dimension 240×200 and another original T2-weighted image with dimension 480×360 . They have the same slice thickness of 7.5mm and consists of 25 slices. Both data from BrainCare are without perceived distortion.

2.2. Geo-spatial model of MRI volume data

The slices that constitute an MRI volume data are assumed to be enclosed in a hypothetical

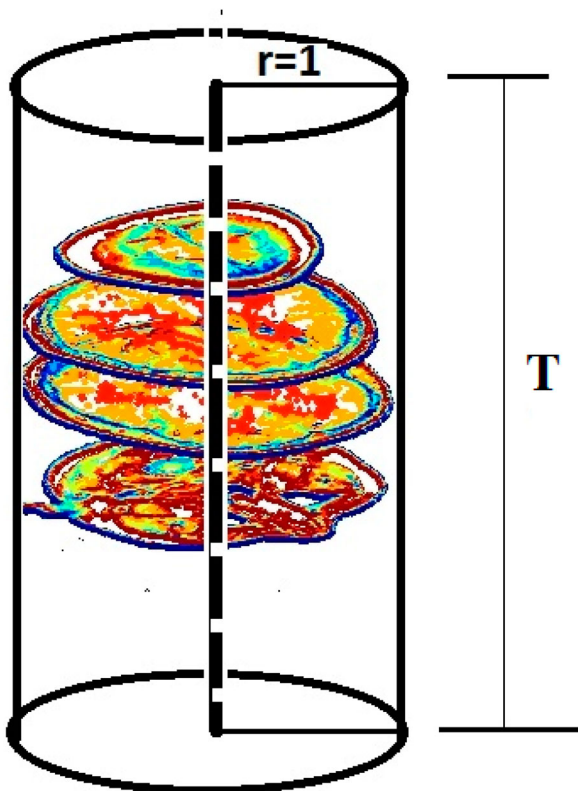


Figure 1. Each MRI slice in an MRI volume is transformed from the original cartesian coordinate system to cylindrical coordinate system of unit radius $r=1$ and height T .

geographic region (\mathbf{s}) as described by a 3D cylindrical coordinate system of unit radius and height T shown in Figure 1:

$$\mathbf{s} = \{r, \theta, t \mid 0 \leq r \leq 1, -\pi \leq \theta \leq \pi, 1 \leq t \leq T\} \in \mathbf{R}^3 \quad (1)$$

where r and θ are the radial and angular distances of pixel locations in the foreground of each slice, respectively. The geographic region is regionalized as shown in Figure 2 by patching each slice into $Q=4$ equal angular segments

$$\theta_q = \left\{ \left(-\pi + (q-1) \frac{2\pi}{Q} \right) < \theta < \left(\pi + (q-Q) \left(\frac{2\pi}{Q} \right) \right) \right\}, \quad (2)$$

where $q = \{1, 2, \dots, Q\}$.

2.3. Modeling experiment

There are seven steps in the modelling experiment. The outcome of the modelling experiment shows three separate Gaussian distributed quality models. Graphical description of the modelling experiment can be explained using the flow chart in Figure 3.

2.3.1. Foreground extraction

Foreground function **FR** extracts foreground image **FI** from each slice image **TIM** in each of the 250 MRI volume data.

2.3.2. Local entropy filtering

Local entropy feature image **LEI** is extracted from each slice using local entropy filter **ENF** of size 3×3 .

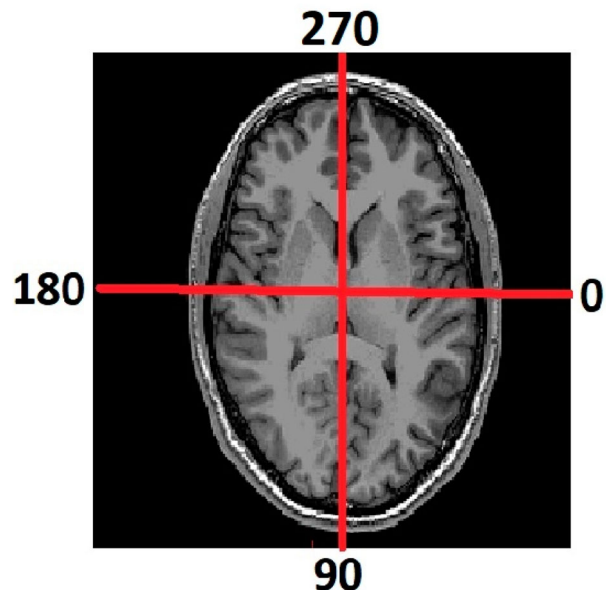


Figure 2. The red lines demarcate an MRI slice into four equal angular segments.

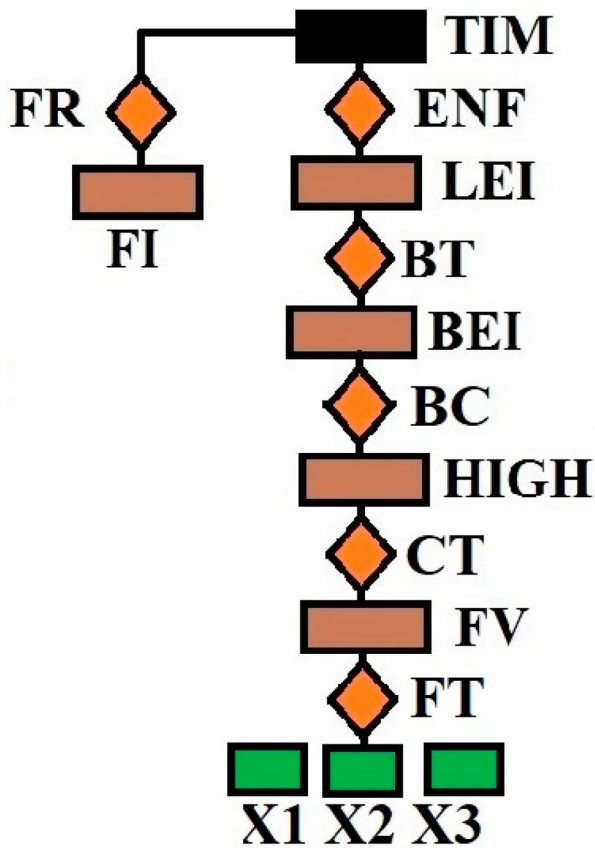


Figure 3. Flow chart of the modelling experiment. Foreground **FI** of a model image **TIM** in the database is extracted **FR**. An entropy filter **ENF** filters each image in the database. The local entropy image **LEI** is thresholded and transformed **BT** into a binary image **BEI**. The binary image is classified **BC** to extract the high **HIGH** entropy feature image. The high entropy feature image is transformed **CT** from its original cartesian coordinate system to cylindrical coordinate system. Feature vectors extracted **FEX** from all the images in the database are classified into three feature vectors **FV**. The feature vectors are further transformed **FT** into Gaussian distributed quality models; global angular segment pixel density **X1**, transverse angular segment pixel density **X2** and whole brain angular segment pixel density **X3**.

2.3.3. Binary transformation

The mean of the local entropy feature image is determined and used as a global threshold which transforms **BT** the local entropy feature image to a binary image **BEI**

2.3.4. Local entropy classification

Binary classification **BC** extracts the high entropy feature image **HIGH** which represents the structural information in the slice. The pixel density in the high entropy region is determined from the ratio of the number of pixels in the high entropy region to the number of pixels in the foreground.

2.3.5. Coordinate transformation

Pixel locations in the high entropy feature image are transformed **CT** from the classical cartesian coordinate

system to cylindrical coordinate system. The pixel locations are further segmented into four equal angular segments as shown in Figure 2. Angular pixel density is the ratio of the number of high entropy pixels in each angular segment to the total number of foreground pixels.

2.3.6. Feature extraction

Three feature vectors **FV** are extracted from all the slices in each MRI volume data. They are whole brain angular segment pixel density **X1**, transverse segment pixel density **X2** and whole brain pixel density **X3**.

- (1) *Whole Brain Angular Segment Pixel Density X1.* This feature vector is derived from each angular segment in a slice. Specific angular pixel density corresponding to all the slices is summed and averaged to obtain a 1×4 feature vector for each MRI volume data.
- (2) *Transverse Segment Pixel Density X2.* Variations in brain size across subjects within a population such as the ADNI database is the result of variation in the number of useful slices in each MRI volume data. Transverse segment pixel density is invariant to these variations. Invariance property is attained by arranging successive axial slices into four sets where each set contains, as much as possible, equal number of slices. Pixel density derived from the high entropy region in each group is summed and averaged to obtain a 1×4 transverse segment pixel density for an MRI volume data.
- (3) *Whole Brain Pixel Density X3.* It is derived from the pixel density of the high entropy feature image for each slice. The pixel density for the high entropy region in all the slices in a volume data are summed and averaged to obtain the whole brain pixel density for a volume data.

2.3.7. Quality models

Each feature vector extracted from an MRI volume data are defined within a finite interval, $\{0 \leq x \leq 1\}$. Furthermore, each feature vector can be regarded as a random variable drawn from each of the 250 MRI volume data in the model database. Their mean and variance are finite. According to the central limit theorem, the distribution will tend to a Gaussian [46–48]. Figure 4 shows five histogram distributions of the whole brain pixel density feature vector fitted with normal data. Each distribution was derived from 50, 100, 150, 200 and 250 MRI volume data. We choose to transform histogram distribution of each feature vector based on 250 MRI volume data into quality model, because it potentially captures, as much as possible, the structural information

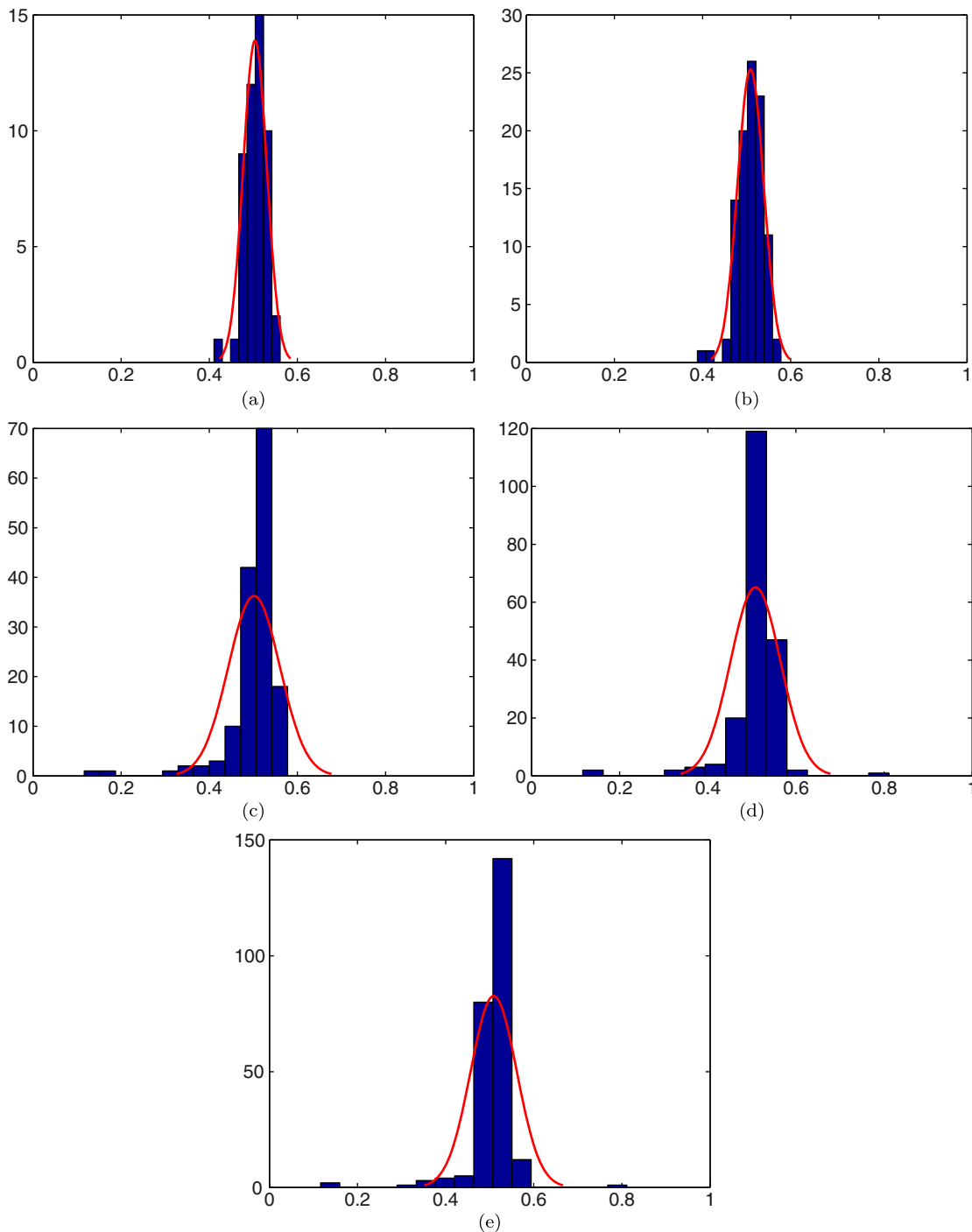


Figure 4. Histogram distribution of the feature vectors extracted from MRI volume data and fitted with normal distribution. The plots were derived from (a) 50, (b) 100, (c) 150, (d) 200 and (e) 250 MRI volume data.

across age, gender and race. The three quality models were named after the feature vectors: whole brain angular segment pixel density X_1 , transverse segment pixel density X_2 and whole brain pixel density X_3 . The mean value for the low and the high entropy areas for the whole brain pixel density are 0.4734 and 0.5471, respectively. This is in agreement with the results reported in [49] for the grey matter, white matter and cerebrospinal fluids. The Gaussian distributions for each feature model were centred at the mean of the random variables. The standard

deviation was estimated using the principle of three-sigma rule [50].

2.4. System operation

The algorithm was implemented in the MatLab computing environment. The flow chart in Figure 5 and the images displayed in Figure 6 explain how our proposed method predicts image quality. The test image TIM in Figure 6(a) is rotated by 180 degrees as shown in Figure 6(b) so as to be in the same orientation as

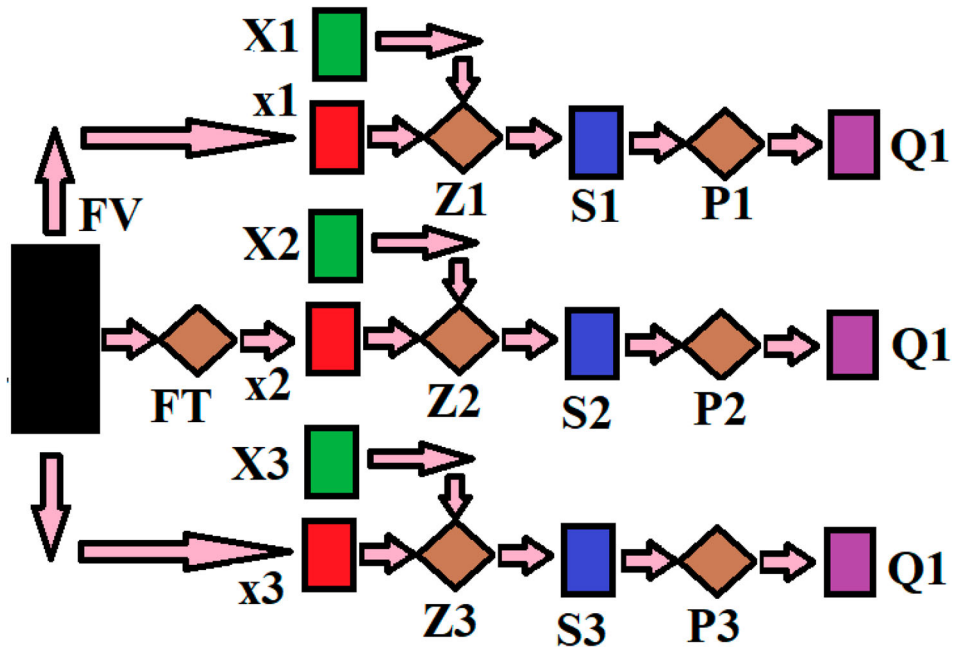


Figure 5. The flow chart of our proposed method for quality evaluation of brain MRI images. Feature vector **FV** extracted from a test image is transformed **FT** to three separate random variable **x1**, **x2** and **x3**. These random variables are used to standardize **Z1**, **Z2**, **Z3** corresponding Gaussian distributed quality model **X1**, **X2**, **X3** which gives normally distributed quality models **S1**, **S2**, **S3**. Cumulative probability distribution **P1**, **P2**, **P3** for each standardized score gives corresponding quality scores **Q1**, **Q2**, **Q3**.

the model images in the image database. Foreground extracted from the rotated image is shown in Figure 6(c). Local entropy feature image of the test image computed using a 3×3 local entropy filter is shown in Figure 6(d). Figure 6(e,f) show the low and the high entropy regions extracted from the local entropy feature image by binarization using the mean of the local entropy feature image as global threshold. Three geospatial feature vectors are extracted **FEX** from the high entropy feature images of the slices in the MRI volume data. The feature vectors are whole brain angular segment pixel density **x1**, transverse segment pixel density **x2** and whole brain pixel density **x3**. Each feature vector is used to standardize **Z1**, **Z2**, **Z3** corresponding Gaussian distributed quality model **X1**, **X2**, **X3** which were derived during the modelling experiment. This gives three corresponding standard scores **S1**, **S2**, **S3** and normal distributions:

$$\begin{aligned} z_1 &= \frac{x_1 - X_1}{\sigma_{X_1}} \\ z_2 &= \frac{x_2 - X_2}{\sigma_{X_2}} \\ z_3 &= \frac{x_3 - X_3}{\sigma_{X_3}} \end{aligned} \quad (3)$$

where σ_{X_1} , σ_{X_2} and σ_{X_3} are the estimate of the standard deviation for each quality model.

Cumulative distribution function **P1**, **P2**, **P3** for each standardized score gives corresponding three quality

scores **Q1**, **Q2**, **Q3** of the test image:

$$Q_1 = \begin{cases} 2[P(z_1 \leq X_1)] & \text{if } P(z_1 \leq X_1) \leq 0.5 \\ 2(1 - [P(z_1 \leq X_1)]) & \text{otherwise} \end{cases} \quad (4)$$

$$Q_2 = \begin{cases} 2[P(z_2 \leq X_2)] & \text{if } P(z_2 \leq X_2) \leq 0.5 \\ 2(1 - [P(z_2 \leq X_2)]) & \text{otherwise} \end{cases} \quad (5)$$

$$Q_3 = \begin{cases} 2[P(z_3 \leq X_3)] & \text{if } P(z_3 \leq X_3) \leq 0.5 \\ 2(1 - [P(z_3 \leq X_3)]) & \text{otherwise} \end{cases} \quad (6)$$

The whole brain angular segment pixel density quality score, transverse segment pixel density quality score and the whole brain pixel density quality score are displayed in Figure 6(g)–(i). The whole brain pixel density quality score expresses the quality score of individual slices in the MRI volume data.

3. Experimental results

Quality evaluation was carried out on the test images in their original state and in their noisy and blurred versions. Two separate and identical Gaussian noise levels were generated to simulate the real and imaginary components in the complex plane of MRI acquisition process. Rician noise was added to the data by computing the magnitude of the complex data. The Rician noise level was based on the maximum pixel intensity level of the test image [51]. The noise levels range from 0 % to 9%. Motion blur was induced on a data by convolving it with a special filter that approximates the linear motion of a camera. The linear motion

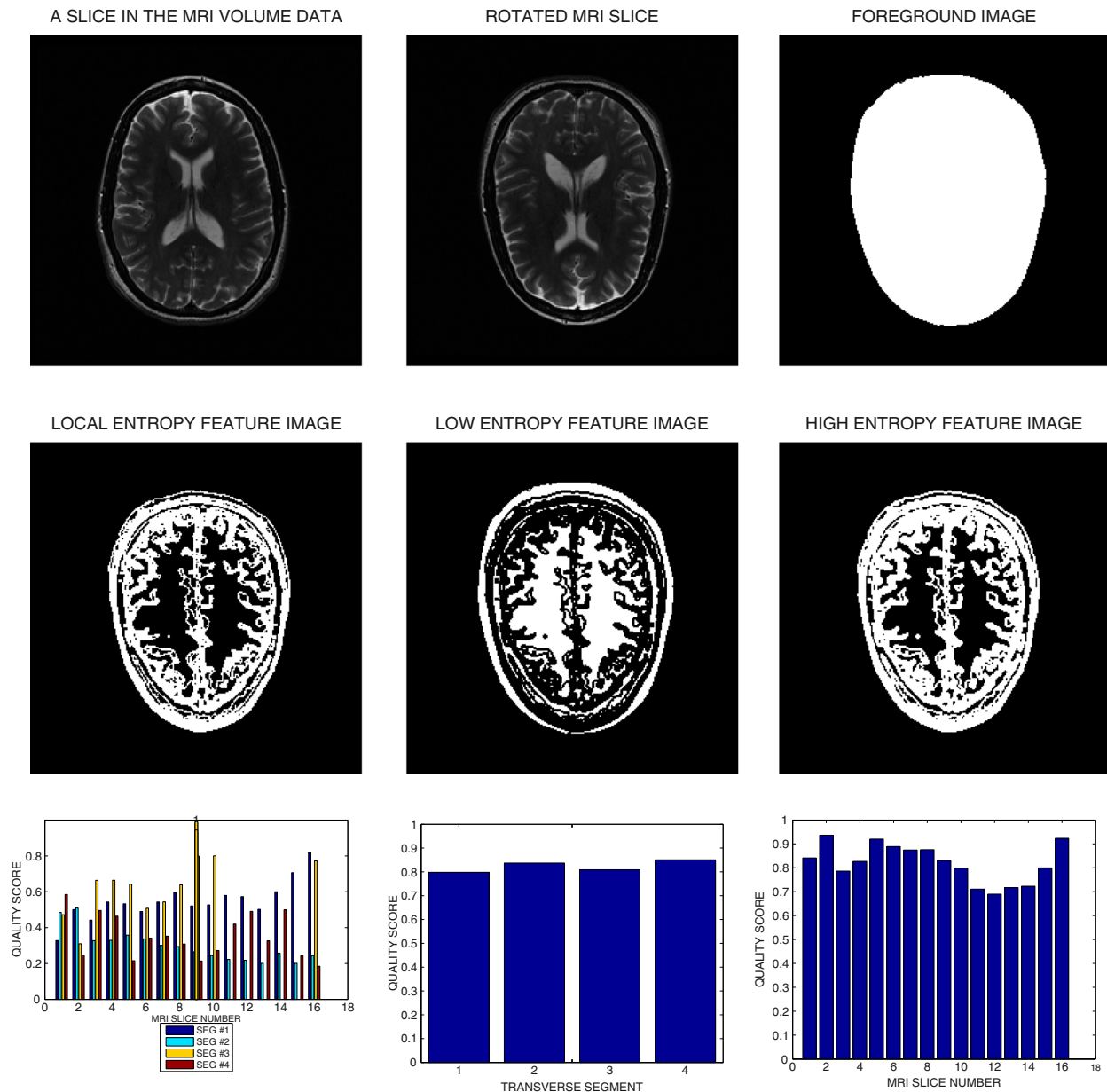


Figure 6. The different stages of post-acquisition quality evaluation for structural brain MRI images. (a) Each slice in the MRI volume data is (b) rotated by 180 degrees to align with the model images in the database. (c) The foreground is extracted followed by (d) filtering to derive the local entropy image. (e) Thresholding the local entropy image extracts (e) the low entropy feature image and the (f) high entropy feature image (g) Whole brain angular segment pixel density (h) Transverse segment pixel density and (i) Whole brain pixel density, quality scores for sixteen successive slices in the MRI volume data.

is described by two parameters, the linear distance in pixels and the angular distance in degree as defined in [52]. Both parameters were scaled from 1 to 15.

3.1. T2 MRI volume data without perceived distortion

Quality evaluation results for T2-weighted MRI volume data from BrainCare are displayed in Figure 7. Peri-ventricular and white matter lesions are visible in the slices shown in Figure 7(a)–(c). The whole brain angular segment pixel density, transverse segment pixel density and whole brain pixel density quality scores for 10 successive slices in the MRI volume data are displayed in Figure 7(d)–(f), respectively.

3.2. FLAIR MRI volume data without perceived distortion

Figure 8(a)–(c) are slices in a FLAIR volume data from NeuroRx. The whole brain angular segment pixel density, transverse segment pixel density and whole brain pixel density quality scores are displayed in Figure 8(d)–(f), respectively.

3.3. Motion blur degradation

The image in Figure 9(a) is one of the 60 slices in the T2-weighted MRI volume data from NeuroRx. The image in Figure 9(b) is the same image in Figure 9(a) but degraded by motion blur level=5. The blur level on

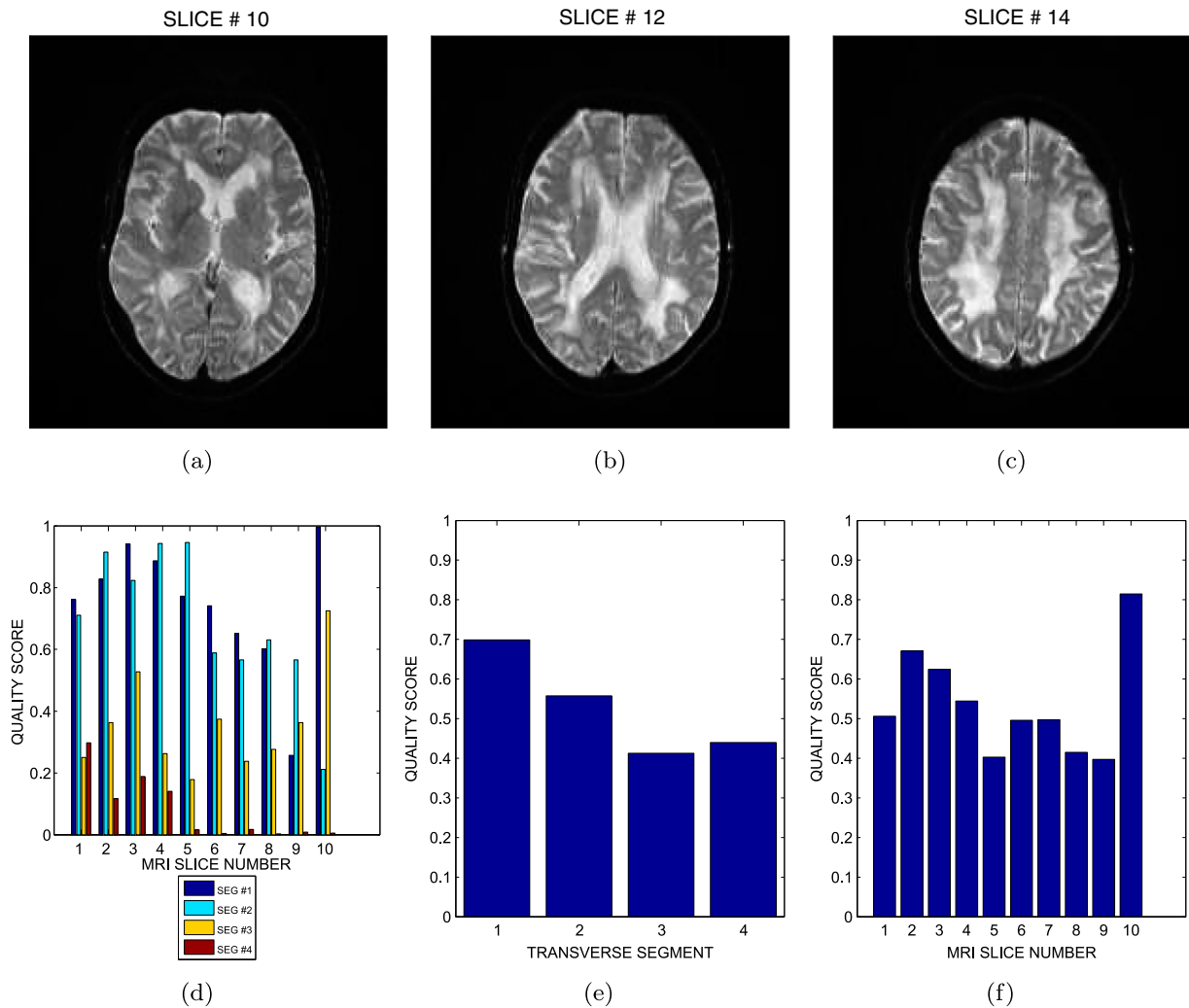


Figure 7. (a), (b), (c) Three T2-weighted slices in the MRI volume data from BrainCare. (d) Whole brain angular segment pixel density (e) Transverse segment pixel density (f) Whole brain pixel density, quality scores for ten successive slices in the volume data.

the same image is significantly increased to 10 and 15 as shown in Figure 9(c,d). Whole brain angular segment pixel density, transverse segment pixel density and whole brain pixel density quality scores of the MRI volume data for blur levels from 1 to 15 are displayed in Figure 9(e)–(g), respectively.

3.4. Noise degradation

Figure 10(a) shows a slice in a T2-weighted MRI volume data without perceived distortion from BrainCare. The same slice in Figure 10(a) is shown in Figure 10(b)–(d) with 4%, 7% and 9% levels of Rician noise. Whole brain angular segment pixel density, transverse segment pixel density and whole brain pixel density quality scores for different levels of Rician noise are displayed in Figure 10(e)–(g), respectively.

3.5. Intensity inhomogeneity

Figure 11 demonstrates quality evaluation on T1-weighted MRI volume data from NeuroRx. The MRI volume data were acquired with different

configurations of intensity inhomogeneity. Six slices in the MRI volume data are displayed in Figure 11(a)–(f). Whole brain angular segment pixel density, transverse segment pixel density and whole brain pixel density quality scores are displayed in Figure 11(g)–(i), respectively.

4. Discussion

4.1. Focus towards region-of-interest

Our proposed method assess image quality at three levels of spatial information. In the first level, the image quality is predicted from each whole slice in the MRI volume data. This is expressed by the whole brain pixel density quality score for each slice. Whole brain pixel density quality score for the MRI volume data is predicted from the average of the whole brain pixel density quality scores for all the slices in the MRI volume data.

The next level of spatial information assigns equal number of successive axial slices in an MRI volume data into four separate groups and assigns quality

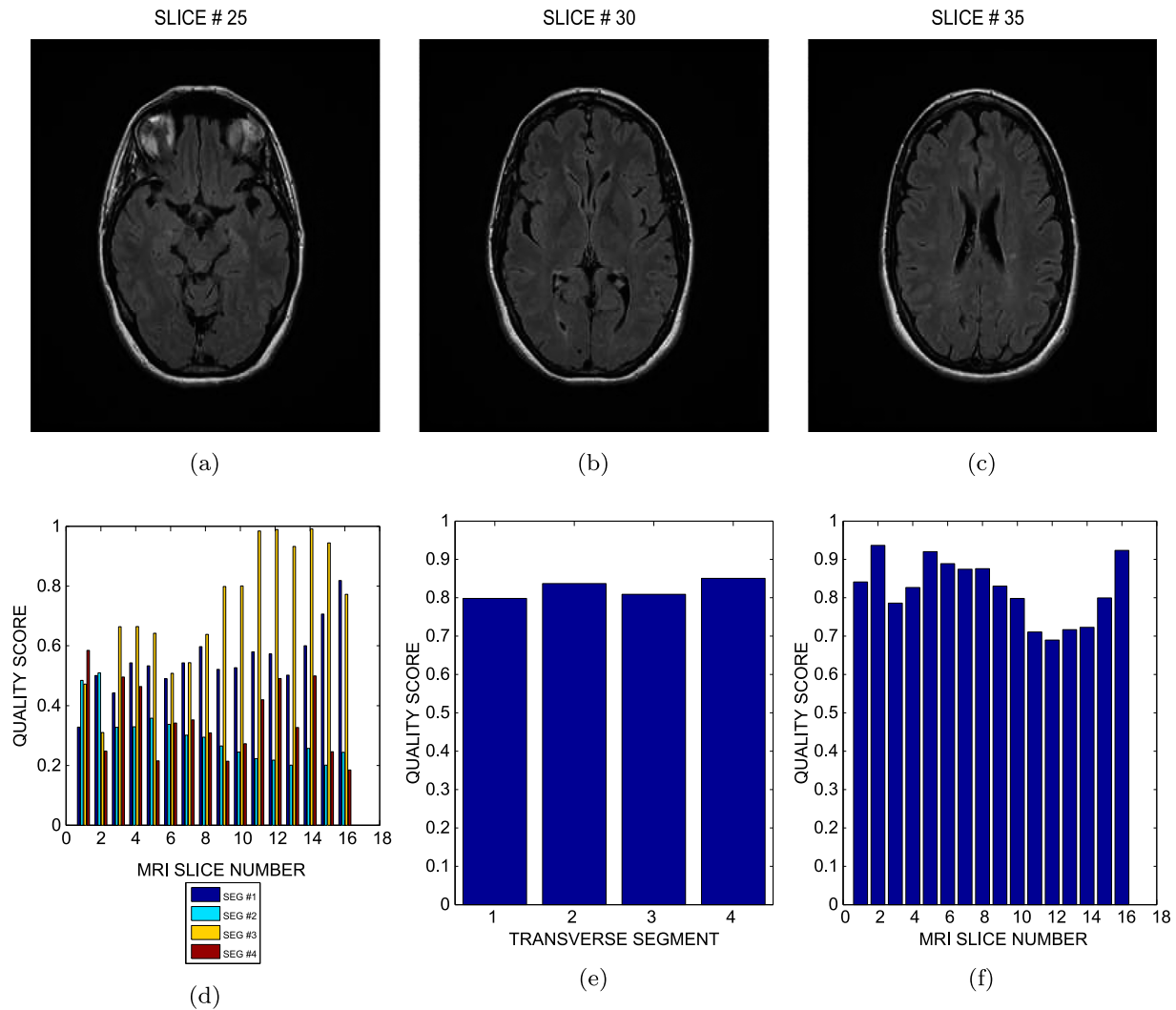


Figure 8. (a), (b), (c) Three FLAIR slices in the MRI volume data from NeuroRx. d) Whole brain angular segment pixel density (e) Transverse segment pixel density (f) Whole brain pixel density, quality scores for sixteen successive slices in the volume data.

score to each group. The quality score is referred to as transverse segment quality score.

The third level of spatial information is the whole brain angular segment pixel density. Each slice in an MRI volume data is partitioned into four equal angular segments. Quality score is assigned to each segment in a slice. Whole brain angular segment quality score is predicted from the average of a specific angular segment across slices in the MRI volume data. The third level of spatial information encourages focus towards region of interest, as combinations of angular segments can describe specific geographic region of the brain. The two angular segments that lie from 180° through 270° to 360° describe the frontal lobe of the brain. The remaining two angular segments that lie between 0° and 180° cover the region described by the parietal lobe of the brain. Furthermore, the two angular segments that span 270° through 360° or 0° to 90° are the left hemisphere of the brain, while the right hemisphere is the region described by the angular segments from 90° through 180° to 270° .

4.2. Correlation across images with acceptable quality

The plots in Figures 6–8 show that our proposed method can fairly predict the quality of slices in an MRI volume data. The whole brain pixel density quality score in Figures 6(i), 7(f) and 8(f) expresses the quality scores of individual slices in the MRI volume data. Since these images under investigation are without any perceived distortion, our proposed method can be said to reveal the variations in image quality between individual slices in an MRI volume data. Average whole brain pixel density quality scores of 0.9, 0.5 and 0.8 predicted for the MRI volume data in Figures 6–8 are in agreement with the status of acceptable quality assigned to the test images.

4.3. Correlation with variations in image quality

Our proposed method can objectively differentiate images having different levels of image quality. Quality prediction shown in Figure 9(e)–(g) for

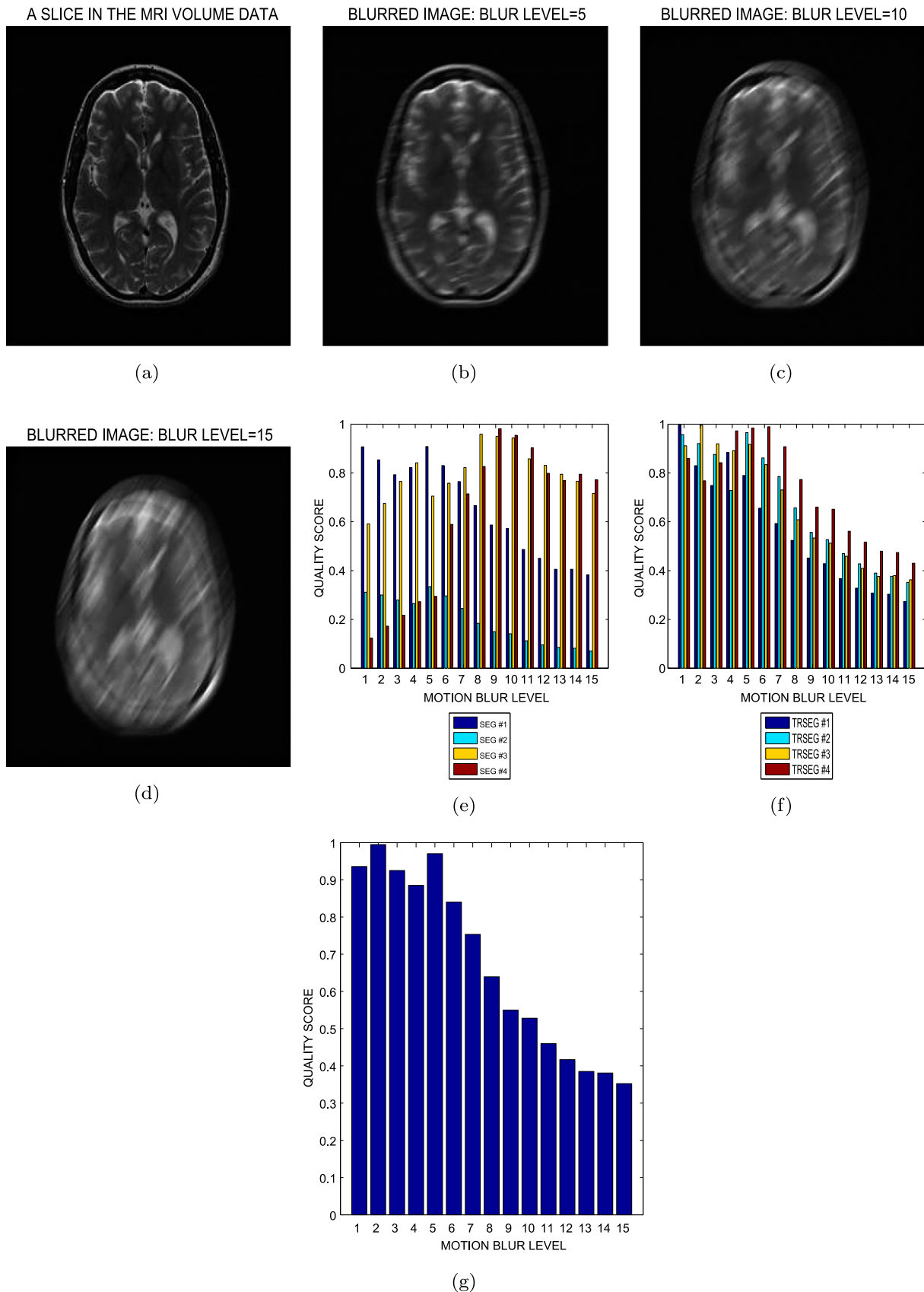


Figure 9. (a) A slice in an MRI volume data from NeuroRx is without any perceived distortion. Each slice in the MRI volume is degraded with 15 different levels of motion blur. Three degraded versions of the slice shown in (a); 5, 10 and 15 levels of motion blur are displayed in (b), (c) and (d), respectively. (e) Whole brain angular segment pixel density (f) Transverse segment pixel density (g) Whole brain pixel density, quality scores for the different levels of motion blur.

motion blur degradation and Figure 10(e)–(g) for Rician noise degradation show correlation between quality index predicted by our proposed method and the

different levels of degradation. In Figure 9(g), the predicted image quality varies from 0.9 to 0.3 for successive blur degradation which varies from 1 to 15. The

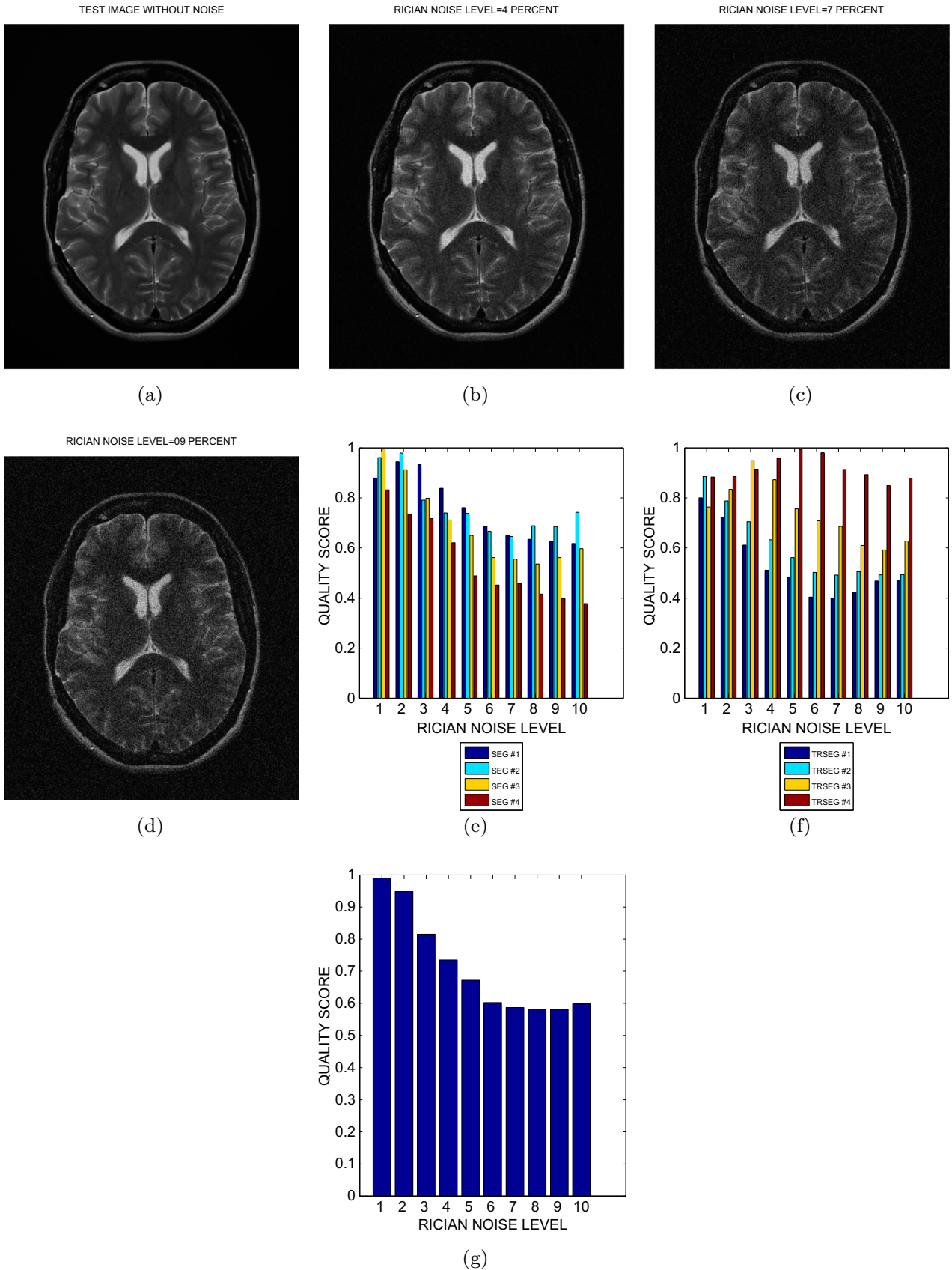


Figure 10. (a) A slice in an MRI volume data from BrainCare is without any perceived distortion. Each slice in the MRI volume data is degraded with ten different levels of Rician noise. Three degraded versions of the slice shown in (a); 2%, 7% and 9% Rician noise are shown in (b), (c) and (d), respectively. (e) Whole brain angular segment pixel density. (f) Transverse segment pixel density. (g) Whole brain pixel density, quality scores for the different levels of noise.

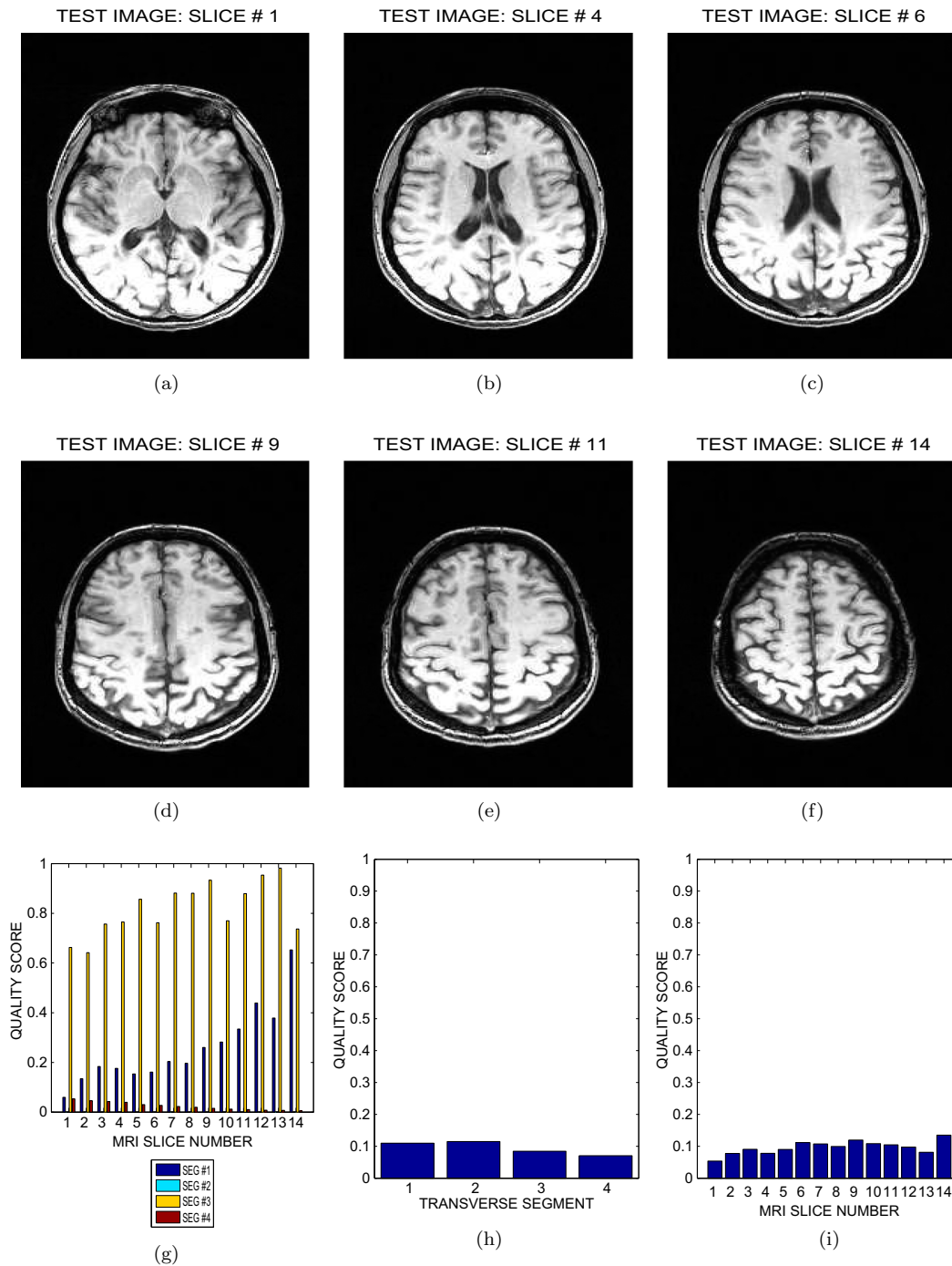


Figure 11. (a) Six slices in a T1-weighted MRI volume data from NeuroRx. The images were originally acquired with intensity inhomogeneity. (e) Whole brain angular segment pixel density. (f) Transverse segment pixel density. (g) Whole brain pixel density, quality scores for 14 successive slices in the MRI volume data.

plots in Figure 10(g) also show correlation between predicted quality scores that varies from 0.95 to 0.6 and the different levels of Rician noise which varies from 0 to 9%.

4.4. Incorporation of fidelity, usefulness and naturalness

The design philosophy behind our proposed method incorporate fidelity, usefulness and naturalness. The usefulness is derived from the use of brain MRI data

from subjects across age, gender and race to build quality models. The fidelity property comes from comparing a test data with the quality models. The naturalness is derived by the use of local entropy filter to describe spatial correlation between constituent anatomic structures.

4.5. Interpretation of proposed quality score

The interpretation of quality score predicted by our proposed method is based on the probability scale.

Thus we recommend quality score threshold of 0.4 to determine if a slice is of acceptable quality or without acceptable quality.

4.6. Absence of comparative performance evaluation

Image quality evaluation methods proposed for a general class of images will require significant modification before they can be applied for quality evaluation of medical images including brain images [53]. Existing quality evaluation methods adopt different distortion models. Our proposed method is based on a quality model that is different from the quality models adopted by existing quality evaluation methods for brain MRI images. There are many definitions of PSNR, SNR and MSE, which makes it difficult to compare quality measures from different imaging systems, modalities and researchers [54]. Performance evaluation results reported in the literature are both model and data dependent, because the different techniques are evaluated on different types of image data [55]. These factors make it difficult for us to carry out comparative performance evaluation of our proposed method.

5. Conclusion

In this report, we propose a new method to evaluate the quality of brain MRI images. It is based on the use of entropy to encode classical image quality attributes. Geo-spatial statistics of local entropy features exploit the geometric similarity of human anatomy across age, gender and race to build three quality models from model images provided by ADNI. A MRI image is evaluated based on how its extracted feature compares with a corresponding quality model. Our proposed method incorporates directional information and spatial dependencies of anatomic structures and this encourages image quality evaluation based on region-of-interest. Quality measures account for structures such as the cortical grey matter and the contrast between the constituent anatomical structures. Based on the test data and the performance evaluation of our proposed method, we are optimistic that our proposed method can be used for quality evaluation in clinical research organizations to assess longitudinal brain MRI images acquired from different scanners and different clinical trial sites. In the future, we intend to acquire more test data for performance evaluation on more types of distortion such as geometric distortion, slice thickness deviation, slice non-uniformity and high-contrast spatial resolution. Future work will also include subjective evaluation by radiologists in the performance evaluation.

Acknowledgments

ADNI is funded by the National Institute on Aging, the National Institute of Biomedical Imaging and Bioengineering, and through generous contributions from the following: AbbVie, Alzheimer's Association; Alzheimer's Drug Discovery Foundation; Araclon Biotech; BioClinica, Inc.; Biogen; Bristol-Myers Squibb Company; CereSpir, Inc.; Cogstate; Eisai Inc.; Elan Pharmaceuticals, Inc.; Eli Lilly and Company; EuroImmun; F. Hoffmann- La Roche Ltd and its affiliated company Genentech, Inc.; Fujirebio; GE Healthcare; IXICO Ltd.; Janssen Alzheimer Immunotherapy Research & Development, LLC.; Johnson & Johnson Pharmaceutical Research & Development LLC.; Lumosity; Lundbeck; Merck & Co., Inc.; Meso Scale Diagnostics, LLC.; NeuroRx Research; Neurotrack Technologies; Novartis Pharmaceuticals Corporation; Pfizer Inc.; Piramal Imaging; Servier; Takeda Pharmaceutical Company; and Transition Therapeutics. The Canadian Institutes of Health Research is providing funds to support ADNI clinical sites in Canada. Private sector contributions are facilitated by the Foundation for the National Institutes of Health (www.fnih.org). The grantee organization is the Northern California Institute for Research and Education, and the study is coordinated by the Alzheimer's Therapeutic Research Institute at the University of Southern California. ADNI data are disseminated by the Laboratory for Neuro Imaging at the University of Southern California.

Marius Pedersen was supported by the Research Council of Norway, project no. 247689 IQMED: Image Quality enhancement in MEDical diagnosis, monitoring and treatment.

Disclosure statement

No potential conflict of interest was reported by the authors.

Funding

Data collection and sharing for this project was funded by the Alzheimer's Disease Neuroimaging Initiative (ADNI) (National Institutes of Health Grant U01 AG024904) and DOD ADNI (Department of Defense award number W81XWH-12-2-0012). Norges Forskningsråd (247689).

Notes on Contributors

M. E. Osadebey obtained a master's degree with distinction in biomedical engineering from Tampere University of Technology, Finland in 2009 and a Ph.D. in engineering and computer science from Concordia University, Montreal, Canada in 2015. His Ph.D. study focused on the processing of MRI images of the brain. Michael is an MRI reader at NeuroRx Research Inc, a Montreal-based clinical research organization. Michael Osadebey duties at NeuroRx include application of advanced image analysis software in the reading of MRI data of neurological diseases patients undergoing clinical trial drug treatment.

Marius Pedersen received his bachelor's degree in Computer Engineering in 2006, and MiT in Media Technology in 2007, both from Gjøvik University College, Norway. He completed a Ph.D. program in colour imaging in 2011 from the University of Oslo, Norway, sponsored by Oce. He is currently employed as an associate professor at NTNU Gjøvik, Norway. He is also the director of the Norwegian Colour and Visual Computing

Laboratory (Colourlab). His work is centred on subjective and objective image quality.

Douglas Arnold is the Director of Magnetic Resonance Spectroscopy Lab, McGill University, Montreal, Canada and the President/CEO of NeuroRx research Inc., a Montreal-based clinical research organization. Arnold is a neurologist with special expertise in MRI. His personal research interests are centred on the use of advanced neuro-imaging techniques to assess the pathological evolution of multiple sclerosis and Alzheimer's disease and to quantify the effects of therapy on these diseases.

Katrina Wendel-Mitoraj obtained her Ph.D. in biomedical engineering from Tampere University of Technology in 2010. Her Ph.D. study focused on electroencephalography (EEG) electrode sensitivity distributions. Katrina is the CEO and founder of BrainCare Oy. BrainCare Oy (<http://braincare.fi/>) is a Tampere University of Technology spin-off company founded in 2013 to deliver personalized solutions to improve the quality of life of epilepsy patients. The organization recently concluded clinical trials for a novel mobile application and supporting solutions for long-term monitoring for epileptic patients.

References

- [1] Pedersen M, Zheng Y, Hardeberg J. Evaluation of image quality metrics for color prints. In: Heyden A, Kahl F, editors. *Image analysis*. Berlin: Springer; 2011. p. 317–326. (Lecture Notes in Computer Science; Vol. 6688).
- [2] Pedersen M, Bonnier N, Hardeberg JY, et al., Attributes of image quality for color prints. *J Electron Imag*. 2010;19(1):011016.
- [3] Wang Z, Bovik A. Modern image quality assessment. Morgan & Claypool; 2006. DOI:10.2200/S00010ED1V01Y200508IVM003
- [4] Janssen R. Computational image quality. Society of Photo Optical. Bellingham, WA: SPIE Press; 2001. (Press Monographs).
- [5] Mansoor AB, Anwar A, Khan S. Subjective evaluation of image quality measures for white noise and gaussian blur-distorted images. *Imag Sci J*. 2013;61(1):13–21.
- [6] Duvernoy HM. The human brain: surface, three-dimensional sectional anatomy with MRI, and blood supply. Vienna: Springer Science & Business Media; 2012.
- [7] Mori S, Wakana S, Van Zijl PC, et al., MRI atlas of human white matter. Vol. 16. Amsterdam: American Society of Neuroradiology; 2005.
- [8] Frisoni GB, Fox NC, Jack CR, et al., The clinical use of structural MRI in alzheimer disease. *Nat Rev Neurol*. 2010;6(2):67–77.
- [9] Scheltens P, Leys D, Barkhof F, et al., Atrophy of medial temporal lobes on MRI in 'probable' Alzheimer's disease and normal ageing: diagnostic value and neuropsychological correlates. *J Neurol, Neurosurg Psychiatry*. 1992;55(10):967–972.
- [10] Arnold DL, Calabresi PA, Kieseier BC, et al., Effect of peginterferon beta-1a on MRI measures and achieving no evidence of disease activity: results from a randomized controlled trial in relapsing-remitting multiple sclerosis. *BMC Neurol*. 2014;14(1):777–0.
- [11] Selmaj K, Kappos L, Arnold D, et al., Safety and tolerability results from the decide study: A phase 3 active-comparator study of daclizumab hyp in relapsing-remitting multiple sclerosis (p7.230). *Neurology*. 2015;84(14 Supplement):P7.230.
- [12] Comi G, Cohen J, Arnold D, et al., Efficacy results of the phase 2 portion of the radiance trial: a randomized, double-blind, placebo-controlled trial of oral rpc1063 in adults with relapsing multiple sclerosis (p7.198). *Neurology*. 2015;84(14 Supplement):P7.198.
- [13] Yalman Y, Akar F, Bayilmis C. A web-based digital analysis interface for image quality assessment. *Imag Sci J*. 2014;62(3):149–160.
- [14] Wang Z, Bovik AC, Sheikh HR, et al., Image quality assessment: from error visibility to structural similarity. *IEEE Trans Image Process*. 2004;13(4):600–612.
- [15] Narwaria M, Lin W. Objective image quality assessment based on support vector regression. *IEEE Trans Neural Netw*. 2010 Mar;21(3):515–519.
- [16] Prieto F, Guarini M, Tejos C, et al., Metrics for quantifying the quality of MR images. In: Proceedings of the 17th Annual Meeting of ISMRM; Honolulu, Hawaii; 2009. p. 4696.
- [17] Miao J, Huang F, Narayan S, et al., A new perceptual difference model for diagnostically relevant quantitative image quality evaluation: A preliminary study. *Magn Reson Imag*. 2013;31(4):596–603.
- [18] Miao J, Huo D, Wilson DL. Quantitative image quality evaluation of MR images using perceptual difference models. *Med Phys*. 2008;35(6):2541–2553.
- [19] ul Haque MI, Qadri MT, Siddiqui N. Reduced reference blockiness and blurriness meter for image quality assessment. *Imag Sci J*. 2015;63(5):296–302.
- [20] Woodard JP, Carley-Spencer MP. No-reference image quality metrics for structural MRI. *Neuroinformatics*. 2006;4(3):243–262.
- [21] Mittal A, Moorthy AK, Bovik AC. No-reference image quality assessment in the spatial domain. *IEEE Trans Image Process*. 2012 Dec;21(12):4695–4708.
- [22] Fang Y, Ma K, Wang Z, et al., No-reference quality assessment of contrast-distorted images based on natural scene statistics. *IEEE Signal Process Lett*. 2015 Jul;22(7):838–842.
- [23] Mortamet B, Bernstein MA, Jack CR, et al., Automatic quality assessment in structural brain magnetic resonance imaging. *Magn Reson Med*. 2009;62(2):365–372.
- [24] Saad MA, Bovik AC, Charrier C. Blind image quality assessment: a natural scene statistics approach in the DCT domain. *IEEE Trans Image Process*. 2012;21(8):3339–3352.
- [25] Kim WG, Kwon OJ, Pang HS. Wavelet-based distortion measure for binary images. *Imag Sci J*. 2013;61(5):408–418.
- [26] Sinha N, Ramakrishnan AG. Quality assessment in magnetic resonance images. *Crit RevTM Biomed Eng*. 2010;38(2):127–141.
- [27] Pedersen M, Hardeberg JY. Full-reference image quality metrics: classification and evaluation. *Foundations Trends Comput Graph Vis*. 2012;7(1):1–80.
- [28] Pedersen M. Evaluation of 60 full-reference image quality metrics on the CID: IQ. In: 2015 IEEE International Conference on Image Processing, ICIP 2015, Quebec City, QC, Canada, September 27–30, 2015; 2015. p. 1588–1592.
- [29] Cavaro-Menard C, Zhang L, Le Callet P. Diagnostic quality assessment of medical images: challenges and trends. In: 2010 2nd European Workshop on Visual Information Processing (EUVIP); July; 2010. p. 277–284.
- [30] Thung KH, Raveendran P. A survey of image quality measures. In: 2009 International Conference for Technical Postgraduates (TECHPOS); Kuala Lumpur, Malaysia; Dec; 2009. p. 1–4.
- [31] Moraru L, Moldovanu SS, Obreja CD. A survey over image quality analysis techniques for brain MR images. *Int J Radiol*. 2015;2(1):24–28.

- [32] Chandler DM. Seven challenges in image quality assessment: past, present, and future research. *ISRN Signal Processing*. 2013.
- [33] Wang Z. Objective image quality assessment: facing the real-world challenges. In: *Society for Imaging Science and Technology, International Symposium on Electronic Imaging, Image Quality and System Performance XII*; 2016. p. 1–6.
- [34] Lee JC, Su Y, Tu TM, et al., A novel approach to image quality assessment in iris recognition systems. *Imag Sci J*. 2010;58(3):136–145.
- [35] Cressie N. *Statistics for spatial data*. New York: John Wiley & Sons; 2015.
- [36] Colliot O, Camara O, Dewynter R, et al., Description of brain internal structures by means of spatial relations for MR image segmentation. In: Fitzpatrick M, Sonka, M, editors. *Medical Imaging 2004*. San Diego, CA: International Society for Optics and Photonics; 2004. p. 444–455.
- [37] Bowden DM, Martin RF. Neuronames brain hierarchy. *Neuroimage*. 1995;2(1):63–83.
- [38] Osadebey M, Pedersen M, Arnold D, et al., Bayesian framework inspired no-reference region-of-interest quality measure for brain MRI images. *J Med Imag*. 2017;4(2):025504–025504.
- [39] Wendel K, Osadebey M, Malmivuo J. Incorporating craniofacial anthropometry into realistically-shaped head models. In: Dössel O, Schlegel W, editors. *World congress on medical physics and biomedical engineering*; September 7–12, 2009; Munich, Germany. Berlin: Springer; 2010. p. 1706–1709. (IFMBE Proceedings; Vol. 25/4).
- [40] Osadebey M. Simulation of realistic head geometry using radial vector representation of magnetic resonance image data [master's thesis]. Tampereen teknillinen yliopisto. Julkaisu-Tampere University of Technology; 2009.
- [41] Wendel KE. The influence of tissue conductivity and head geometry on eeg measurement sensitivity distributions [dissertation]. Tampereen teknillinen yliopisto. Julkaisu-Tampere University of Technology; 2010.
- [42] Shiee N, Bazin PL, Cuzzocreo JL, et al., Reconstruction of the human cerebral cortex robust to white matter lesions: method and validation. *Human Brain Mapp*. 2014;35(7):3385–3401.
- [43] Mugler JP, Brookeman JR. Three-dimensional magnetization-prepared rapid gradient-echo imaging (3d mp rage). *Magn Reson Med*. 1990;15(1):152–157.
- [44] Reimer P, Meaney JF, Parizel PM, et al., *Clinical MR imaging*. Berlin: Springer; 2010.
- [45] Jack CR, Bernstein MA, Fox NC, et al., The alzheimer's disease neuroimaging initiative (adni): MRI methods. *J Magn Reson Imag*. 2008;27(4):685–691.
- [46] Ruderman DL. The statistics of natural images. *Network: Comput Neural Syst*. 1994;5(4):517–548.
- [47] Leon-Garcia A. *Probability, statistics and random processes for electrical engineering*. 3rd ed. Upper Saddle River (NJ): Prentice-Hall, Pearson Education Inc.; 2008. Chapter 3.
- [48] Norman G, Streiner D. *Biostatistics: the bare essentials*. 3rd ed. Hamilton: People's Medical Publishing House; 2008. Chapter 4.
- [49] Lüders E, Steinmetz H, Jäncke L. Brain size and grey matter volume in the healthy human brain. *Neuroreport*. 2002;13(17):2371–2374.
- [50] Grafarend EW. *Linear and nonlinear models: fixed effects, random effects, and mixed models*. Berlin: Walter de Gruyter; 2006.
- [51] Coupé P, Manjón JV, Gedamu E, et al., Robust Rician noise estimation for MR images. *Med Image Anal*. 2010;14(4):483–493.
- [52] Deshpande AM, Patnaik S. A novel modified cepstral based technique for blind estimation of motion blur. *Optik-Int J Light Electron Opt*. 2014;125(2):606–615.
- [53] Chow LS, Paramesran R. Review of medical image quality assessment. *Biomed Signal Process Control*. 2016;27:145–154.
- [54] Kupinski MA, Barrett HH. *Small-animal spect imaging*. Vol. 233. New York: Springer; 2005.
- [55] Vovk U, Pernus F, Likar B. A review of methods for correction of intensity inhomogeneity in MRI. *IEEE Trans Med Imag*. 2007;26(3):405–421.